Applied Energy 384 (2025) 125412

Contents lists available at ScienceDirect

Applied Energy

journal homepage: www.elsevier.com/locate/apenergy

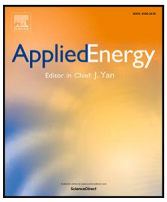

Cost-effective scheduling of a hydrogen-based iron and steel plant powered by a grid-assisted renewable energy system

Pengfei Su [a], Yue Zhou [a,*], Hongyi Li [b], Hector D. Perez [c], Jianzhong Wu [a]

[a] School of Engineering, Cardiff University, Cardiff, CF24 3AA, UK
[b] Department of Electrical and Computer Engineering, Iowa State University, Ames, IA 50011, USA
[c] Department of Chemical Engineering, Carnegie Mellon University, Pittsburgh, PA 15213, USA

GRAPHICAL ABSTRACT

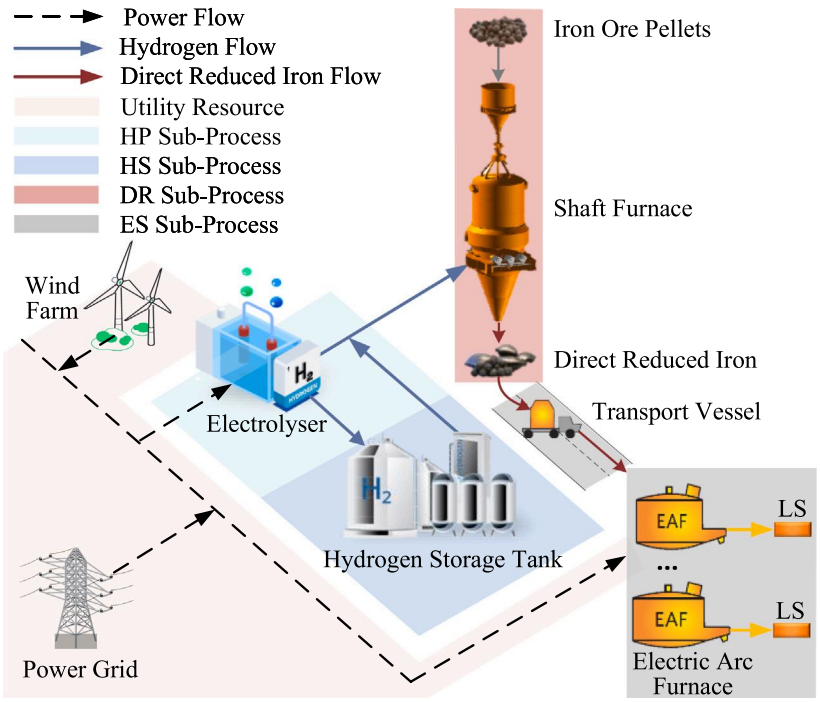

ARTICLE INFO

Dataset link: 10.17035/cardiff.28359110

Keywords:
Hydrogen-based iron and steel plant
Integrated resource-task network
Grid-assisted renewable energy system

ABSTRACT

The iron and steel industry contributes approximately 25% of global industrial CO_2 emissions, necessitating substantial decarbonisation efforts. Hydrogen-based iron and steel plants (HISPs), which utilise hydrogen-based direct reduction of iron ore followed by electric arc furnace steelmaking, have attracted substantial research interest. However, commercialisation of HISPs faces economic feasibility issues due to the high electricity costs of hydrogen production. To improve economic feasibility, HISPs are jointly powered by local renewable generators and bulk power grid, i.e., by a grid-assisted renewable energy system. Given the

* Corresponding author.
E-mail address: zhouy68@cardiff.ac.uk (Y. Zhou).

https://doi.org/10.1016/j.apenergy.2025.125412
Received 20 October 2024; Received in revised form 4 January 2025; Accepted 20 January 2025
Available online 9 February 2025

Scheduling optimisation

variability of renewable energy generation and time-dependent electricity prices, flexible scheduling of HISP production tasks is essential to reduce electricity costs. However, cost-effectively scheduling of HISP production tasks is non-trivial, as it is subject to critical operational constraints, arising from the tight coupling and distinct operational characteristics of HISPs sub-processes. To address the above issues, this paper proposes an integrated resource-task network (RTN) to elaborately model the critical operational constraints, such as resource balance, task execution, and transfer time. More specifically, each sub-process is first modelled as an individual RTN, which is then seamlessly integrated through boundary dependency constraints. By embedding the formulated operational constraints into optimisation, a cost-effective scheduling model is developed for HISPs powered by the grid-assisted renewable energy system. Numerical results demonstrate that, compared to conventional scheduling approaches, the proposed method significantly reduces total operational costs across various production scales.

1. Introduction

The highly energy-intensive iron and steel industry (ISI) currently accounts for approximately 25% of global industrial CO_2 emissions in 2019 and requires significant decarbonisation efforts for climate-change mitigation [1]. Despite progress in emission reductions through efficiency improvement and waste valorisation [2], decarbonisation efforts remain insufficient to meet ISI's climate commitments, which highlights the need for deep decarbonisation technologies [3,4]. As one of the leading deep decarbonisation routes, the hydrogen (H_2)-based iron and steel plant (HISP), which utilises the H_2-based direct reduction of iron ore (DRI) followed by the electric arc furnace (EAF) steelmaking (H_2-DRI-EAF) process, has garnered increasing attention. There have been intensive industrial investments [5] and successful pilot projects, such as those of Swedish forerunners [6], in this area.

Nonetheless, commercialisation of HISP still faces economic feasibility challenges due to the high electricity costs associated with hydrogen production [2]. Consequently, numerous recent studies have focused on methods to enhance the HISP economic feasibility, such as configuring energy sources [2], selecting optimal plant locations [4], and designing regional supply chains [7]. A consensus has emerged that co-locating manufacturing processes with a local renewable energy source (RES)-dominated electricity supplies, supplemented by grid assistance, can achieve higher energy efficiency and cost reduction [8]. Currently, power grid is not fully decarbonised due to its reliance on a mix of renewable and non-renewable energy sources. This varied energy mix results in fluctuations in electricity prices and grid-related emissions. Therefore, flexible scheduling of HISP production tasks is essential for reducing electricity costs in response to the variability of renewable energy generation and time-dependent electricity prices and grid-related emissions [7]. By emphasising a cost-effective scheduling model, economic feasibility can be enhanced without significant additional investments.

Recent studies have underscored the significant role of cost-effective scheduling in achieving substantial cost savings and improving grid support in energy-intensive industries. In the context of cost savings, Papadaskalopoulos et al. [9] develops a whole-system model that evaluates the economic benefits of the industrial demand flexibility. Their model optimises both long-term investments and short-term operations while accounting for the variability in RES generations. Similarly, Zhang et al. [10] propose scheduling models for steel plants, in order to minimise electricity costs by exploiting the operational flexibility of electric arc furnaces (EAF). Gan et al. [11] further investigate demand-side management strategies to reduce electricity purchases in steel plants through targeted adjustments to key energy-intensive production processes. Additionally, Huang et al. [12] introduce a real-time demand response framework based on hour-ahead electricity pricing. This approach combines artificial neural networks for price forecasting with mixed-integer linear programming to optimise energy consumption without compromising production goals. Beyond cost savings considerations, several studies have explored the role of industrial facilities in enhancing grid stability. For example, Zhou et al. [13] examine industrial heating loads such as bitumen tanks for their potential to provide frequency response services through decentralised control systems. Zhao et al. [14] propose a hierarchical control strategy that integrates thermostatically controlled loads and hydrogen energy storage systems to strengthen frequency regulation. Furthermore, Palensky et al. [15] advocate for a holistic approach to demand-side management that integrates technological innovation, behavioural adjustments, and market-based incentives to improve both grid efficiency and stability.

However, cost-effective scheduling of HISP production tasks is non-trivial, as it subjects to critical operational constraints. The challenges of formulating operational constraints stem from the tight coupling and distinct operational characteristics of HISP sub-processes. Traditional simulation tools, such as HYSYS, ProSim, and Aspen Plus, are commonly used for simulating industrial processes and optimising operational parameters. However, these tools often fall short in systemic decision optimisation and tend to overlook intricate dependencies among production tasks [16,17]. Similarly, while some studies have assessed the economic feasibility and environmental impact of HISP for long-term techno-economic evaluations [7,18], they neglect operational constraints and complex dependencies among production tasks, potentially resulting in infeasible schedules [17]. In recent years, the application of Artificial Intelligence (AI) techniques has significantly increased in enhancing steel production efficiency. For instance, studies utilising reinforcement learning have demonstrated the ability of AI to manage complex production operations and improve overall performance [19–21]. However, conventional "black-box" AI models suffer from high data requirements and insufficient interpretability, limiting their industrial applications. As an alternative , Resource-Task Network (RTN) method, originally proposed within the Process System Engineering community, offers a promising for industrial applications where transparency, interpretability and clear constraint management are emphasised.

The RTN approach, firstly proposed in 1994 [22], is a modelling framework to mathematically depict the allocation of resources to tasks, ensuring well-organised resource utilisation and task scheduling. Thus, RTN is recognised as one of the most general and powerful paradigms for process scheduling, and has been widely adopted to handle complex processes with multiple stages and critical production requirements [23]. The RTN paradigm guarantees interpretability and transparency by representing the fundamental governing rules of industrial processes through algebraic constraints [22]. The resulting algebraic constraints can be mathematically formulated as mixed integer programming (MIP) problems and then solved using MIP solvers to generate optimal schedules.

A few attempts have been made by researchers to apply RTN method to iron and steel production processes, which mainly focus on the scrap-based EAF steelmaking process and the blast furnace-basic oxygen furnace (BF-BOF) process. For scrap-based EAF steelmaking process, Castro et al. [24] validate the effectiveness of RTN formulation of the scrap-based EAF steelmaking process, capturing the key operational constraints of an EAF steel plant. Based on this work, Zhang et al. [10] expand the RTN formulation to include EAF flexibility by adjusting power rates, thus further reducing electricity costs. In response to rising energy costs and decarbonisation pressures in the ISI, Su et al. [25] extend the RTN formulation that incorporates both

Nomenclature

Acronyms

ISI	Iron and steel industry
HISP	Hydrogen-based iron and steel plan
H_2	Hydrogen
DRI	Direct reduction of iron ore
EAF	Electric arc furnace
H_2-DRI-EAF	Hydrogen-based direct reduction of iron ore followed by the electric arc furnace
RES	Renewable energy source
AI	Artificial intelligence
RTN	Resource-task network
MIP	Mixed integer programming
BF-BOF	Blast furnace-basic oxygen furnace
HP	Hydrogen production
HS	Hydrogen storage
HR	Hydrogen release
DR	Direct reduction
ES	Electric arc furnace steelmaking
PEMEL	Proton exchange membrane electrolyser
SF	Shaft furnace
HT	Hydrogen tanks
LS	Liquid steel
TV	Transport vessels
OPT	Overall production time
WE	Water electrolysis
WT	Wind turbine
PG	Power grid
SoHC	State of the hydrogen charge

Sets

$\mathcal{T}$	Time index set $\{1, 2, \dots, \mathrm{T}\}$
$\mathcal{H}$	Heat product set $\{1, 2, \dots, \mathrm{H}\}$
$\mathcal{R}^{\mathrm{HP}}$	Set of resources in hydrogen production sub-process
$\mathcal{R}^{\mathrm{HS}}$	Set of resources in hydrogen storage sub-process
$\mathcal{R}^{\mathrm{DR}}$	Set of resources in direct reduction sub-process
$\mathcal{R}^{\mathrm{ES}}$	Set of resources in EAF steelmaking sub-process
$\mathcal{R}^{\mathrm{Util}}$	Set of utility resources
$\mathcal{I}^{\mathrm{HP}}$	Set of tasks in hydrogen production sub-process
$\mathcal{I}^{\mathrm{HS}}$	Set of tasks in hydrogen storage sub-process
$\mathcal{I}^{\mathrm{DR}}$	Set of tasks in direct reduction sub-process
$\mathcal{I}^{\mathrm{ES}}$	Set of tasks in EAF steelmaking sub-process

Subscripts

t	The time index in the uniform time grid
θ	The relative time index corresponds to the start of the task
h	Heat referring to a batch of molten metal
$\mathrm{Eq}^{\mathrm{Elz}}$	Equipment resource representing the PEMEL
$\mathrm{H}_2^{\mathrm{DC}}$	Material resource representing H_2 directly consumed by DR process
$\mathrm{H}_2^{\mathrm{TP}}$	Material resource representing total production of hydrogen
$\mathrm{Eq}^{\mathrm{HT}}$	Equipment resource representing the hydrogen tank
$\mathrm{H}_2^{\mathrm{St}}$	Material resource representing the hydrogen for being stored
$\mathrm{H}_2^{\mathrm{HT}}$	Material resource representing the hydrogen stored in the hydrogen tank
$\mathrm{H}_2^{\mathrm{Re}}$	Material resource representing the hydrogen for being released
$\mathrm{Eq}^{\mathrm{SF}}$	Equipment resource representing the shaft furnace
$\mathrm{H}_2^{\mathrm{De}}$	Material resource representing the hydrogen demand in the DR process
$\mathrm{DRI}^{\mathrm{TP}}$	Material resource representing the DRI produced in the DR process
DR	Task representing direct reduction activity
$\mathrm{Eq}^{\mathrm{TV}}$	Equipment resource representing the transport vessel
$\mathrm{Eq}^{\mathrm{EAF}}$	Equipment resource representing the electric arc furnace
$\mathrm{DRI}^{\mathrm{De}}$	Material resource representing the DRI demand in the ES process
$\mathrm{DRI}_{\mathrm{h}}^{\mathrm{d}}$	Material resource representing the intermediate product of the heat h located at the transfer destination (superscript d)
LS_{h}	Material resource representing the LS product of the heat h
WE	Processing task representing water electrolysis activity
HS	Processing task representing hydrogen storage activity
HR	Processing task representing hydrogen release activity
Tr_{h}	Transporting task representing transporting activity for the $\mathrm{DRI}_{\mathrm{h}}^{\mathrm{d}}$
ES_{h}	Processing task representing ES activity for the $\mathrm{DRI}_{\mathrm{h}}^{\mathrm{d}}$
$\mathrm{El}^{\mathrm{Elz}}$	Utility resource representing electricity demand of PEMEL
$\mathrm{El}^{\mathrm{EAF}}$	Utility resource representing electricity demand of EAF
$\mathrm{El}^{\mathrm{WT}}$	Utility resource representing electricity generation of WT
$\mathrm{El}^{\mathrm{PG}}$	Utility resource representing electricity purchased from power grid
$\mathrm{Em}^{\mathrm{PG}}$	Utility resource representing indirect emissions

Parameters

δ	Duration of each time slot
$\overline{\omega}_t^{E,\mathrm{Buy}}$	Wholesale electricity prices at time t
$\overline{\omega}_t^{E,\mathrm{Cur}}$	Penalty price for curtailment of wind power at time t
$\overline{c}_t^{\mathrm{CI}}$	Grid-related carbon intensity at time t
$\overline{\omega}^{C}$	Carbon tax rate
$\overline{LS_{TD}}$	Total demand for liquid steel
$\overline{\mu}_{r,i,t}$	Discrete consumption/production ratio of resource r in task i at time t
$\overline{\nu}_{r,i,t}$	Variable consumption/production ratio of resource r in task i at time t
$\overline{\kappa}_{\mathrm{DRI}}^{\mathrm{De}}$	The amount of DRI transferred in one batch (ton)
$\overline{W}_{\mathrm{Tr}}, \overline{\omega}_{\mathrm{Tr}}$	Maximum and minimum transfer time of DRI (min)
$\overline{Eq^{\mathrm{Elz}}}^{L/U}$	Lower/upper bounds of the quantities of Eq^{Elz}
$\overline{Eq^{\mathrm{HT}}}^{L/U}$	Lower/upper bounds of the quantities of Eq^{HT}
$\overline{Eq^{\mathrm{SF}}}^{L/U}$	Lower/upper bounds of the quantities of Eq^{SF}

$\overline{\underline{Eq^{\mathrm{TV}}}}^{L/U}$	Lower/upper bounds of the quantities of Eq^{TV}
$\overline{\underline{Eq^{\mathrm{EAF}}}}^{L/U}$	Lower/upper bounds of the quantities of Eq^{EAF}
$\overline{\underline{H_2^{\mathrm{HT}}}}^{L/U}$	Lower/upper bounds of the H_2 flow capacity of HT
$\overline{\underline{El^{\mathrm{Trans}}}}^{L/U}$	Lower/upper capacity limit of transmission power line
$\overline{\underline{H^{\mathrm{WE}}}}^{L/U}$	Lower/upper bounds of operational capacities for task WE
$\overline{\underline{H^{\mathrm{HS}}}}^{L/U}$	Lower/upper bounds of operational capacities for task HS
$\overline{\underline{H^{\mathrm{HR}}}}^{L/U}$	Lower/upper bounds of operational capacities for task HR
$\overline{\mathrm{DRI}}$	Constant DRI production capacity (ton)
$\overline{\mathrm{EAF}}$	Constant EAF production capacity (ton)

Variables

$R_{r,t}$	Resource inventory level of resource material r at time t
$N_{i,t}$	Number of times task i is executed at time t
$\xi_{i,t}$	Extent of task i at time t
$\Pi_{r,t}$	External transfer of resource r at time t
ζ	Overall production time required to complete all scheduled tasks
Z_t	Auxiliary binary variable to determine if required demand is met
$P_{\mathrm{El}^{\mathrm{Elz}},t}$	Electricity consumed by PEMEL at time t
$P_{\mathrm{El}^{\mathrm{EAF}},t}$	Electricity consumed by EAF at time t
$P_{\mathrm{El}^{\mathrm{WT}},t}$	Electricity generated by WT at time t
$P_{\mathrm{El}^{\mathrm{PG}},t}$	Electricity purchased from the power grid at time t
$P_t^{G,\mathrm{Elz}}$	Electricity consumed by electrolyser from grid at time t
$P_t^{G,\mathrm{EAF}}$	Electricity consumed by EAF from power grid at time t
$P_t^{\mathrm{WT,Elz}}$	Electricity consumed by PEMEL from WT at time t
$P_t^{\mathrm{WT,EAF}}$	Electricity consumed by EAF from WT at time t
P_t^{Cur}	Curtailed wind generations at time t
$\mathrm{Em}_t^{\mathrm{PG}}$	Indirect emissions at time t

cost and emission considerations. For BF-BOF process, Wang et al. [26] build an RTN formulation of the steelmaking-refinery-continuous casting process, facilitating the schedule of flexible resources at iron and steel sites. Comparing with the steelmaking processes studied in existing literature, the H_2-DRI-EAF process consists of multiple tightly coupled sub-processes with distinct operational constraints. However, conventional RTN methods have limited capability to handle the H_2-DRI-EAF process, calling for the augmentation of RTN formulation. To the authors' best knowledge, the RTN formulations to model the operational constraints of the H_2-DRI-EAF process have not yet been explored.

Given the above research gaps, this study proposes a novel cost-effective scheduling model for HISPs. To capture the distinct operational characteristics, an RTN model is first developed for each HISP sub-process. Individual RTN models are then integrated through boundary dependency constraints, which reflect the coupling of HISP sub-processes. The integrated RTN model is embedded into the optimisation model to support the cost-effective scheduling of HISPs. The main contributions of this paper are threefold:

1. The distinct operational characteristics of each HISP sub-process are analysed and converted to an abstract representation. Atop of the abstract representations, unified mathematical models of HISP sub-processes are developed based on the RTN method, which depict the operational constraints originated from each sub-process.
2. Considering both the task sequence and mass balance, boundary dependency constraints are proposed to model the coupling and interaction between consecutive sub-processes. Based on the boundary dependency, the integrated RTN model of HISP production is developed from individual RTNs, which serves as constraints in the HISP scheduling problem.
3. A cost-effective scheduling model is developed for the HISP, which is powered by a grid-assisted renewable energy system. The proposed scheduling model comprehensively considers the fluctuations in renewable generations, electricity prices, and grid emissions, allowing HISP to fully exploit its flexibility while adhering to critical operational constraints.

The remainder of this paper is organised as follows. Section 2 includes the description of H_2-DRI-EAF process and the analysis of its flexibility potential. Section 3 introduces the RTN representation, and Section 4 provides mathematical formulations of the cost-effective schedule optimisation model of an HISP. Section 5 introduces the case study and presents the result and discussion. Section 6 concludes this paper.

2. Problem statement

The H_2-DRI-EAF process, depicted in Fig. 1, incorporates four co-locating sub-processes: hydrogen production (HP), hydrogen storage (HS), direct reduction (DR), and EAF steelmaking (ES), all powered by a grid-assisted renewable energy system. Firstly, hydrogen is produced by water electrolysis in a proton exchange membrane electrolyser (PEMEL). The hydrogen generated can either be supplied to the shaft furnace (SF) for DR of iron ore pellets into DRI in the SF or stored in hydrogen tanks (HT) for future use. The DRI produced in the SF is then transported to the EAF for further processing into liquid steel (LS) using transport vessels (TV), which are designed to minimise time delays and avoid the need for reheating cooled DRI. Lastly, in the ES sub-process, the DRI undergoes further refinement to remove impurities, resulting in LS production.

Each sub-process in the H_2-DRI-EAF process exhibits distinct operational characteristics and varying degrees of flexibility. The HP sub-process operates continuously, with the ability to adjust power levels based on electricity availability and pricing, thanks to the modular design and voltage control of the PEMEL. Flexibility here arises from both power adjustments and the ability to shift operation times. The HS sub-process, serving as a buffer, provides additional flexibility through hydrogen storage, offering opportunities for arbitrage depending on energy prices and production schedules. In contrast, the DR sub-process has limited electrical flexibility due to its exothermic internal reactions, but introduces constraints into the overall scheduling process. It operates continuously with a constant hydrogen supply rate to maintain a uniform oxidation front, which is critical for stable production [4]. The ES sub-process, operating in batch mode, allows for some scheduling flexibility by adjusting the start times of each batch, but each batch must be processed consistently to maintain product quality. Multiple EAFs are typically used, and their power rates remain constant during the process to ensure consistent liquid steel production.

Conventional scheduling schemes aim to minimise the overall production time (OPT) required to complete all scheduled tasks, which is defined as an optimisation problem as follows:

$$\min \ \zeta, \tag{1}$$

$$\zeta \geq (t-1)\cdot Z_t \cdot \delta, \qquad \forall t \in \mathcal{T}, \tag{2}$$

$$\sum_{t\in\mathcal{T}}\sum_{h\in\mathcal{H}} R_{LS_h,t} \geq \overline{LS_{TD}} \cdot Z_t, \qquad \forall t \in \mathcal{T}, \tag{3}$$

$$\sum_{t\in\mathcal{T}} Z_t = 1, \qquad \forall t \in \mathcal{T}, \tag{4}$$

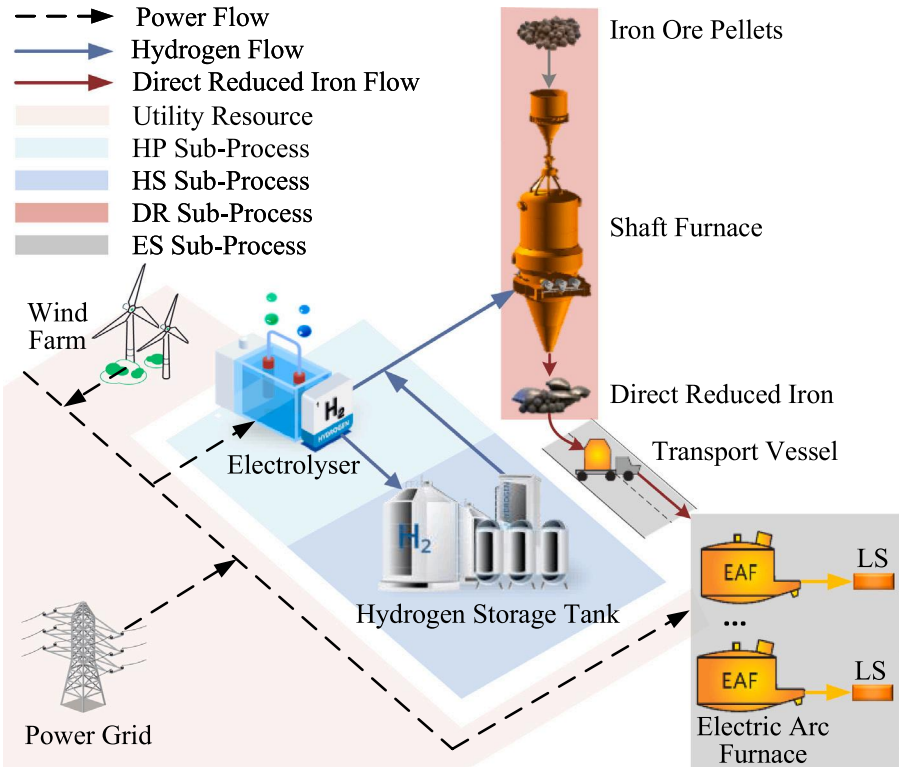

Fig. 1. Typical H_2-DRI-EAF Process. (HP: Hydrogen Production, HS: Hydrogen Storage, DR: Direct Reduction, ES: EAF Steelmaking, LS: Liquid Steel).

and other HISP operational constraints in Section 4.2,

where ζ represents the OPT required to complete all scheduled tasks; Z_t is the auxiliary binary variable showing whether all the LS have been produced, with 1 indicating that the LS has all been produced at the time t and 0 indicating it is not. δ represents the duration of each time slot, measured in minutes. $R_{LS_h,t}$ denotes the amount of resource LS_h at time t; and $\overline{LS_{TD}}$ denotes the total demand for LS. $\mathcal{T}$ is the time index set $\{1,2,\ldots,T\}$. $\mathcal{H}$ is the heat product set $\{1,2,\ldots,H\}$.

Constraint (2) ensures that the OPT is larger than or equal to the completion time required to produce all the final products, i.e. the LS. Since the objective function minimises the OPT, the left hand side of constraint (2) will actually be equal to the right hand side in the end. The OPT is calculated as $(t-1)\cdot Z_t\cdot\delta$, where Z_t is an indicator showing whether all the LS has been produced. When Z_t equals 1, it represents that the LS has all been produced at the time t, and the total time used is calculated as the product of the number of time intervals $(t-1)$ used and the duration δ of each interval. Constraint (3) ensures that the amount of resource LS_h at time t,denoted as $R_{LS_h,t}$, meets the total amount of LS required to be produced, namely $\overline{LS_{TD}}$, whenever the binary indicator Z_t equals 1. This signifies that the LS has all been produced at that point in time. Constraint (4) ensures that the auxiliary binary variable Z_t equals 1 exactly once throughout the entire time horizon $\mathcal{T}$. Other HISP operational constraints will be elaborated in Section 4.2.

Conventional scheduling schemes fail to leverage flexibility in scheduling, particularly in response to fluctuations in energy prices or renewable energy availability, which do not consider cost efficiency. The flexibility within these sub-processes offers opportunities to improve economic feasibility. However, to fully exploit this flexibility, critical operational constraints, such as resource balance, task execution time, and transfer time, must be met.

The challenges in formulating operational constraints arise from two aspects: (1) each HISP sub-process has its distinct operational constraints. For example, HP sub-process operates continuously while the ES sub-process operates discretely; (2) HISP sub-processes are tightly coupled. For example, task sequence and mass balance must be constrained between consecutive sub-processes that are separately modelled. To address these challenges, this paper develops an integrated RTN model for HISP production constraints and embeds it in the cost-effective scheduling, allowing HISP to takes advantage of flexibility in response to fluctuations in renewable energy generation, electricity prices, and grid emissions.

3. Integrated resource task network representation

The integrated RTN representation of the H_2-DRI-EAF process, depicted in Fig. 2, serves as an abstract layer between real plant entities and mathematical model entities. It includes four sub-RTN models: HP-RTN, HS-RTN, DR-RTN, and ES-RTN, each designed for specific sub-process characteristics and interconnected through boundary dependency constraints. The demand and supply of electricity and related grid-related emissions were represented as utility resources. The RTN maps the process into resource nodes (representing equipment or materials) and task nodes (describing processing or transfer operations), with interactions detailing how tasks utilise and transform resources. For an in-depth exploration of how this method applies to representing industrial processes, [23] is recommended.

In this paper, the resources considered in the integrated RTN model encompass resource sets for all sub-RTN models and the utility resource set. In HP-RTN, the resource set $\mathcal{R}^{HP}$, shown in (5), comprises equipment such as the PEMEL $\mathrm{Eq}^{\mathrm{Elz}}$, and materials such as total hydrogen production $\mathrm{H}_2^{\mathrm{TP}}$ in PEMEL and direct hydrogen consumption by the DR process $\mathrm{H}_2^{\mathrm{DC}}$. In HS-RTN, the resource set $\mathcal{R}^{\mathrm{HS}}$, shown in (6), comprises equipment like hydrogen storage tank $\mathrm{Eq}^{\mathrm{HT}}$; materials like hydrogen for being stored $\mathrm{H}_2^{\mathrm{St}}$, hydrogen stored in the hydrogen tank $\mathrm{H}_2^{\mathrm{HT}}$, hydrogen for being released $\mathrm{H}_2^{\mathrm{Re}}$. In DR-RTN, the resource set $\mathcal{R}^{\mathrm{DR}}$, shown in (7), include equipment such as the shaft furnace $\mathrm{Eq}^{\mathrm{SF}}$, and materials including hydrogen demand $\mathrm{H}_2^{\mathrm{De}}$ and total production for DRI in the DR process $\mathrm{DRI}^{\mathrm{TP}}$. In ES-RTN, the resource set $\mathcal{R}^{\mathrm{ES}}$, shown in (8), include equipment such as the transport vessel $\mathrm{Eq}^{\mathrm{TV}}$ and EAF $\mathrm{Eq}^{\mathrm{EAF}}$, and

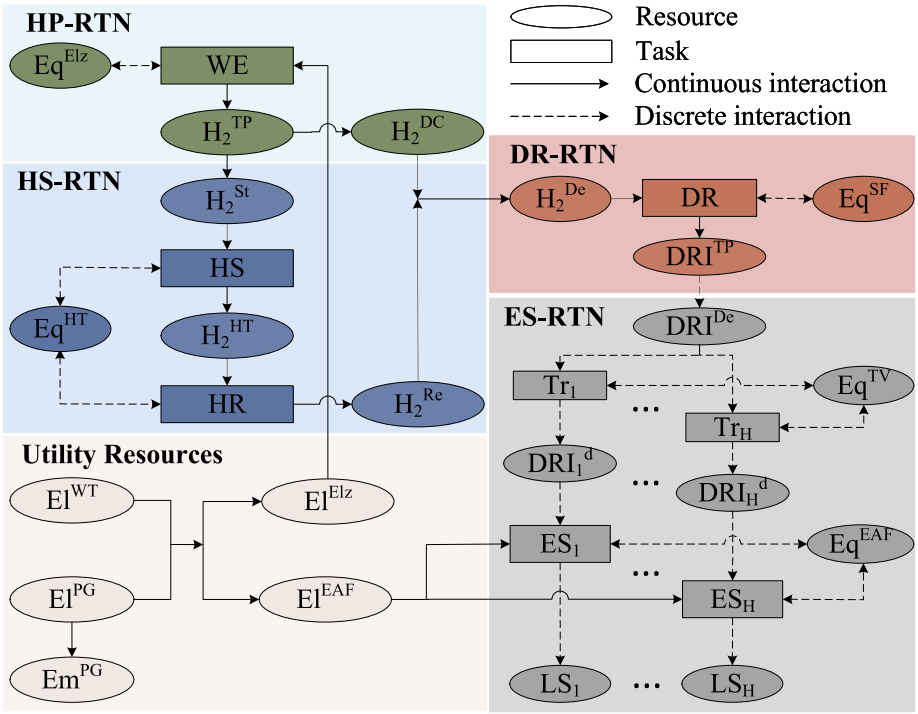

Fig. 2. Integrated RTN Representation of the H_2-DRI-EAF Process.

materials such as DRI demand of the ES process $\mathrm{DRI}^{\mathrm{De}}$, intermediate product DRI at the transfer destination $\mathrm{DRI}_{\mathrm{h}}^{\mathrm{d}}$ and final product LS_{h}. Here, the subscript h refers to an individual batch (also known as "heat" in the iron and steel industry) of molten metal in the batch production process. Multiple heats are produced daily, and each heat is assigned a unique identifier, forming a heat product set $\mathcal{H} = \{1, 2, \ldots, \mathrm{H}\}$. Utility resource set $\mathcal{R}^{\mathrm{Util}}$, shown in (9), include electricity demand of PEMEL $\mathrm{El}^{\mathrm{Elz}}$ and electricity demand of EAF $\mathrm{El}^{\mathrm{EAF}}$, electricity generated by wind turbines $\mathrm{El}^{\mathrm{WT}}$, electricity purchased from power grid $\mathrm{El}^{\mathrm{PG}}$, and indirect emissions $\mathrm{Em}^{\mathrm{PG}}$.

$$\mathcal{R}^{\mathrm{HP}} = \{\mathrm{Eq}^{\mathrm{Elz}}, \mathrm{H}_2^{\mathrm{TP}}, \mathrm{H}_2^{\mathrm{DC}}\}, \tag{5}$$

$$\mathcal{R}^{\mathrm{HS}} = \{\mathrm{Eq}^{\mathrm{HT}}, \mathrm{H}_2^{\mathrm{St}}, \mathrm{H}_2^{\mathrm{Re}}\}, \tag{6}$$

$$\mathcal{R}^{\mathrm{DR}} = \{\mathrm{Eq}^{\mathrm{SF}}, \mathrm{H}_2^{\mathrm{De}}, \mathrm{DRI}^{\mathrm{TP}}\}, \tag{7}$$

$$\mathcal{R}^{\mathrm{ES}} = \{\mathrm{Eq}^{\mathrm{TV}}, \mathrm{Eq}^{\mathrm{EAF}}, \mathrm{DRI}^{\mathrm{De}}, \mathrm{DRI}_h^{\mathrm{d}}, \mathrm{LS}_h \mid \mathrm{h} \in \mathcal{H}\}, \tag{8}$$

$$\mathcal{R}^{Util} = \{\mathrm{El}^{\mathrm{Elz}}, \mathrm{El}^{\mathrm{EAF}}, \mathrm{El}^{\mathrm{WT}}, \mathrm{El}^{\mathrm{PG}}, \mathrm{Em}^{\mathrm{PG}}\}. \tag{9}$$

The tasks considered in the integrated RTN model consist of all task sets for all sub-RTN models. In HP-RTN, the task set $\mathcal{I}^{HP}$, shown in (10), includes the processing task such as the water electrolysis (WE) task WE. In HS-RTN, the task set $\mathcal{I}^{HS}$ shown in (11), encompasses the HS task HS and the H_2 release (HR) task HR. In DR-RTN, the task set $\mathcal{I}^{DR}$, shown in (12), consists of the DR task DR. In ES-RTN, the task set $\mathcal{I}^{ES}$, shown in (13), consists of transfer task Tr_h after the generation of DRI^{De} and the EAF steelmaking (ES) task ES_h of the heat h.

$$\mathcal{I}^{\mathrm{HP}} = \{\mathrm{WE}\}, \tag{10}$$

$$\mathcal{I}^{\mathrm{HS}} = \{\mathrm{HS}, \mathrm{HR}\}, \tag{11}$$

$$\mathcal{I}^{\mathrm{DR}} = \{\mathrm{DR}\}, \tag{12}$$

$$\mathcal{I}^{\mathrm{ES}} = \{\mathrm{Tr}_{\mathrm{h}}, \mathrm{ES}_{\mathrm{h}} \mid \mathrm{h} \in \mathcal{H}\}. \tag{13}$$

The network flow chart in Fig. 2 indicates how each task interacts with each resource, consisting of continuous interaction and discrete interaction. Continuous interactions imply that a task consistently consumes or generates resources throughout its duration. In contrast, discrete interactions imply that a task interacts only at specific points during the task. In continuous operations (i.e., HP, HS, and DR processes), processing tasks interact with equipment resources discretely but with other resources continuously. In a batch operation (i.e., ES process), processing tasks interact only with electricity resources continuously, but interact with other resources discretely.

Detailed interactions are captured by the interaction parameters $\overline{\mu_{r,i,\theta}}$ and $\overline{\nu_{r,i,\theta}}$. These parameters measure the specific increase or decrease of the resource r by task i at the relative time θ—the time occurring θ intervals after the start of task i. The parameter $\overline{\mu_{r,i,\theta}}$ is used for resources consumed in discrete quantities, such as equipment, while $\overline{\nu_{r,i,\theta}}$ is used for resources consumed in variable amounts, such as materials and utilities. The discrete-time representation is employed in the integrated RTN model [22]. Continuous task i is considered a series of discrete tasks, each typically spanning a time interval τ_i. For batch operations such as ES-RTN, the parameter τ_i specifies the duration of the batch task i. Once a batch task begins, the batch task continues uninterrupted for a period equal to τ_i.

In Fig. 3, we illustrate interaction parameters for a WE task with its interactive resources. For simplicity, we discretised continuous tasks into uniform 30-min intervals to match the typical granularity of electricity pricing and renewable energy forecasts. In Fig. 3, there are three distinct time references: t is the index of the uniform time grid; the relative time index θ corresponds to the start of the task; and *Time* represents the actual hour of the day. We assume that the WE task starts when t equals 1. This task involves resources such as Eq^{Elz}, H_2^{TP}, and El^{Elz}. At first, the task decreases Eq^{Elz} by one as it utilises the operation unit; upon completion of the WE process, Eq^{Elz} increases by one as the equipment is freed. Additionally, H_2^{TP} increases within the range between the minimum hydrogen production capacity $\overline{H^{WE}}^{L}$ and the maximum hydrogen production capacity $\overline{H^{WE}}^{U}$, according to the PEMEL power settings. The electricity consumption of the WE task is calculated based on the electricity required per unit of hydrogen, denoted as $\overline{\eta^H}$. Thus, the total power demand for each time interval falls within the range $\left[\overline{H^{WE}}^{L} \cdot \overline{\eta^H}, \overline{H^{WE}}^{U} \cdot \overline{\eta^H}\right]$.

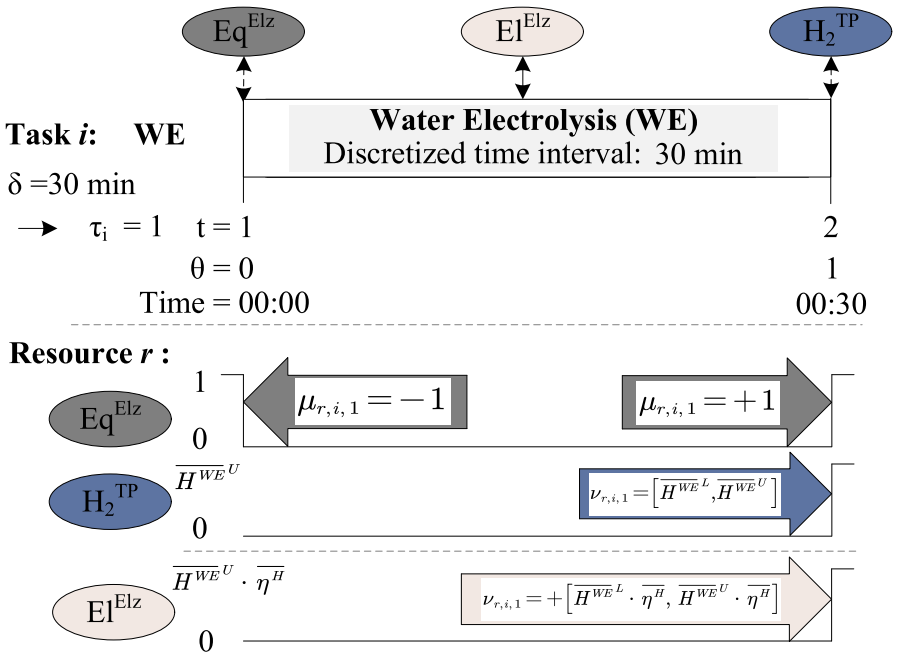

Fig. 3. Illustration of Interaction Parameters for Water Electrolysis Task.

4. Cost-effective scheduling optimisation of a H_2-based steel plant

4.1. Objective functions

The objective function for cost-effective scheduling aims to minimise the day-ahead operation cost minimisation objective over a 24-h period, as described in (14). This objective function consists of three components: (i) the cost of purchasing electricity from the power grid, (ii) the penalty cost associated with the curtailment of renewable energy, and (iii) the indirect emission cost resulting from electricity usage from the power grid.

$$\min \sum_{t\in\mathcal{T}} \left(P_{El^{PG},t} \cdot \overline{\omega}_t^{E,Buy} + P_t^{Cur} \cdot \overline{\omega}_t^{E,Cur} + Em^{PG} \cdot \overline{\omega}^{C} \right) \cdot \Delta t, \tag{14}$$

where $P_{El^{PG},t}$ represents the electricity purchased from the power grid, $\overline{\omega}_t^{E,Buy}$ denotes the day-ahead wholesale electricity prices, P_t^{Cur} indicates the amount of renewable electricity curtailed, $\overline{\omega}_t^{E,Cur}$ is the penalty price for curtailment, $\overline{c}_t^{CI}$ reflects the day-ahead forecast carbon intensity of the power grid, and $\overline{\omega}^{C}$ is the carbon tax.

4.2. Constraints

In this section, operational constraints and power balance constraints are mathematically formulated based on the RTN discrete-time representation in Section 3. [1] Guided by the operational mechanisms of the HISP, operational constraints are mathematically formulated using continuous and discrete variables governed by algebraic inequalities and equalities. [2]

4.2.1. Resource balance

Resource balance constraints manage the interaction between each resource and its relevant tasks over the time horizon, as shown in (15).

$$\boldsymbol{R}_{r,t} = \boldsymbol{R}_{r,t-1} + \sum_{i\in I_r} \sum_{\theta=0}^{\tau_i} \left(\overline{\mu_{r,i,\theta}} \cdot \boldsymbol{N}_{i,t-\theta} + \overline{\nu_{r,i,\theta}} \cdot \xi_{i,t-\theta} \right) + \Pi_{r,t}, \tag{15}$$
$$\forall r \notin \mathcal{R}^{Util},\ \forall t \in \mathcal{T},$$

in which the value $\boldsymbol{R}_{r,t}$ of resource r at time t is equal to its previous value at $t-1$ adjusted by the amounts produced or consumed of that resource by all relevant tasks $\mathcal{I}_r$ in the time range $[t-\tau_i, t]$ or any entrance or exit of the external resource $\Pi_{r,t}$ that moves in or out of the system. Each task is indexed by i, and the binary variable $N_{i,t}$ designates the start of task i at time t, where $N_{i,t} = 1$ means that task i begins at time t. $\xi_{i,t}$ represents the extent of production or consumption by task i at time t. The value of $\Pi_{r,t}$ is deemed positive when a resource enters the system, such as reactants, and negative when it exits the system, such as products.

The electricity demand for PEMEL and EAF is calculated as (16) and (17) respectively. Indirect emissions of the purchased electricity from the power grid is calculated as (18)

$$\boldsymbol{P}_{El^{Elz},t} = \sum_{i\in I^{HP}} \sum_{\theta=0}^{1} \overline{v_{El^{Elz},i,\theta}} \cdot \xi_{i,t-\theta}, \qquad \forall t \in \mathcal{T}, \tag{16}$$

$$\boldsymbol{P}_{El^{EAF},t} = \sum_{i\in I^{ES}} \sum_{\theta=0}^{\tau_i} \overline{v_{El^{EAF},i,\theta}} \cdot \boldsymbol{N}_{i,t-\theta}, \qquad \forall t \in \mathcal{T}, \tag{17}$$

$$Em^{PG} = P_{El^{PG},t} \cdot \overline{c}_t^{CI}, \qquad \forall t \in \mathcal{T}, \tag{18}$$

where $\boldsymbol{P}_{El^{Elz},t}$ and $\boldsymbol{P}_{El^{EAF},t}$ represent the electricity consumption of PEMEL and EAF at each time point t respectively. Furthermore, $\overline{v_{El^{Elz},i,\theta}}$ and $\overline{v_{El^{EAF},i,\theta}}$ denote the variable electricity demand of PEMEL and EAF for the task i at time point t, respectively.

4.2.2. Resource limits

Resource inventories in the H_2-DRI-EAF process are restricted by lower and upper limits, such as limitations of amounts of equipment in all sub-processes shown in (19)–(23), the HT capacity shown in (24), and the transmission line capacity of the power grid shown in (25).

$$\overline{Eq^{Elz}}^{L} \le \boldsymbol{R}_{Eq^{Elz},t} \le \overline{Eq^{Elz}}^{U}, \qquad \forall t \in \mathcal{T}, \tag{19}$$

[1] Constraints in Section 4.2 are critical operational constraints that reflect the standard practices and requirements of the steel plant's daily production processes. In this paper, we assume that the scheduling problem has at least one feasible solution, since the external factors that might lead to model infeasibility are not the primary focuses of this paper.

[2] For plants with unclear operational mechanisms, model learning can be implemented for extracting patterns from observational data to construct the descriptive models. More detail can be found in [27].

$$\overline{Eq^{HT}}^{L} \le \boldsymbol{R}_{Eq^{HT},t} \le \overline{Eq^{HT}}^{U}, \quad \forall t \in \mathcal{T}, \quad (20)$$

$$\overline{Eq^{SF}}^{L} \le \boldsymbol{R}_{Eq^{SF},t} \le \overline{Eq^{SF}}^{U}, \quad \forall t \in \mathcal{T}, \quad (21)$$

$$\overline{Eq^{TV}}^{L} \le \boldsymbol{R}_{Eq^{TV},t} \le \overline{Eq^{TV}}^{U}, \quad \forall t \in \mathcal{T}, \quad (22)$$

$$\overline{Eq^{EAF}}^{L} \le \boldsymbol{R}_{Eq^{EAF},t} \le \overline{Eq^{EAF}}^{U}, \quad \forall t \in \mathcal{T}, \quad (23)$$

$$\overline{H_2^{HT}}^{L} \le \boldsymbol{R}_{H_2^{HT},t} \le \overline{H_2^{HT}}^{U}, \quad \forall t \in \mathcal{T}, \quad (24)$$

$$\overline{El^{Trans}}^{L} \le \boldsymbol{P}_{El^{PG},t} \le \overline{El^{Trans}}^{U}, \quad \forall t \in \mathcal{T}, \quad (25)$$

where $\overline{Eq^{Elz}}^{L/U}$, $\overline{Eq^{HT}}^{L/U}$, $\overline{Eq^{SF}}^{L/U}$, $\overline{Eq^{TV}}^{L/U}$, and $\overline{Eq^{EAF}}^{L/U}$ respectively represent the lower and upper bounds of the quantities of Eq^{Elz}, Eq^{HT}, Eq^{SF}, Eq^{TV}, and Eq^{EAF}. $\overline{H_2^{HT}}^{L/U}$ represents the lower and upper limits of the flow capacity to store and release hydrogen in HT. $\overline{El^{Trans}}^{L/U}$ represents the lower and upper capacity limit of the transmission line.

4.2.3. Task execution

Task execution is limited due to operational capacity limitations. Hydrogen production rate of WE, hydrogen storage and release rates of HT over the time horizon are, respectively, constrained by (26)–(28). Furthermore, simultaneous storage and release from HT are prohibited to prevent inefficiencies and sudden pressure changes, as specified in (29). A common constraint for HT in daily scheduling is that the hydrogen levels at the beginning and end of the day must be equal, as enforced by (30). In DR-RTN, continuous operation with constant DRI production is governed by (31). In ES-RTN, amounts of DRI processed in each batch are governed by (32).

$$\overline{H^{WE}}^{L} \cdot \boldsymbol{N}_{WE,t} \le \xi_{WE,t} \le \overline{H^{WE}}^{U} \cdot \boldsymbol{N}_{WE,t}, \quad \forall t \in \mathcal{T}, \quad (26)$$

$$\overline{H^{HS}}^{L} \cdot \boldsymbol{N}_{HS,t} \le \xi_{HS,t} \le \overline{H^{HS}}^{U} \cdot \boldsymbol{N}_{HS,t}, \quad \forall t \in \mathcal{T}, \quad (27)$$

$$\overline{H^{HR}}^{L} \cdot \boldsymbol{N}_{HR,t} \le \xi_{HR,t} \le \overline{H^{HR}}^{U} \cdot \boldsymbol{N}_{HR,t}, \quad \forall t \in \mathcal{T}, \quad (28)$$

$$\boldsymbol{N}_{HS,t} + \boldsymbol{N}_{HR,t} \le 1, \quad \forall t \in \mathcal{T}, \quad (29)$$

$$\boldsymbol{R}_{H_2^{HT},1} = \boldsymbol{R}_{H_2^{HT},T}, \quad (30)$$

$$\xi_{DR,t} = \overline{DRI} \cdot \boldsymbol{N}_{DR,t}, \quad \forall t \in \mathcal{T}, \quad (31)$$

$$\xi_{EAF,t} = \overline{EAF} \cdot \boldsymbol{N}_{EAF,t}, \quad \forall t \in \mathcal{T}, \quad (32)$$

where $\overline{H^{WE}}^{L/U}$, $\overline{H^{HS}}^{L/U}$ and $\overline{H^{HR}}^{L/U}$ respectively represent the lower and upper bounds of the operational capacities for tasks WE, HS and HR. $\overline{DRI}$ is the constant DRI production capacity in tonnes, and $\overline{EAF}$ is the EAF production capacity in tonnes.

Each batch of DRI is processed in EAF once, as enforced by (33). Similarly, each batch of DRI should be transferred once between DR and ES processes, as enforced by (34).

$$\sum_{t} \boldsymbol{N}_{EAF_h,t} = 1, \quad \forall t \in \mathcal{T}, \forall h \in \mathcal{H}, \quad (33)$$

$$\sum_{t} \boldsymbol{N}_{Tr_h,t} = 1, \quad \forall t \in \mathcal{T}, \forall h \in \mathcal{H}. \quad (34)$$

4.2.4. Transfer time

Hydrogen produced in PEMEL should be either directly utilised by SF for DRI production or stored into HT for hydrogen storage without any waiting time, as enforced by (35). The variable $R_{\mathrm{HT^{TP}},t}$ represents the residual hydrogen available at time t, and can either be zero or a positive value. When $R_{\mathrm{HT^{TP}},t}$ is zero, it indicates that there is no hydrogen waiting at time t. For example, $R_{\mathrm{HT^{TP}},t}$ is set to 0 for all time in (35). This ensures that once the hydrogen $\mathrm{HT^{TP}}$ production is complete by WE task at time t, the subsequent task must start immediately at the same time t to prevent any accumulation in the value of $R_{\mathrm{HT^{TP}},t}$. Similarly, hydrogen must be stored or released from tanks without delay, as enforced by (36) and (37). Hydrogen used in the SF is consumed directly as stipulated by (38), and DRI produced must be transported immediately to prevent production delays, as required by (39). Transfer time limitations are set to prevent cooling effects on hot DRI, potentially compromising quality and increasing reheating costs [10], as specified in (40).

$$\boldsymbol{R}_{H_2^{TP},t} = 0, \quad \forall t \in \mathcal{T}, \quad (35)$$

$$\boldsymbol{R}_{H_2^{St},t} = 0, \quad \forall t \in \mathcal{T}, \quad (36)$$

$$\boldsymbol{R}_{H_2^{Re},t} = 0, \quad \forall t \in \mathcal{T}, \quad (37)$$

$$\boldsymbol{R}_{H_2^{De},t} = 0, \quad \forall t \in \mathcal{T}, \quad (38)$$

$$\boldsymbol{R}_{DRI^{TP},t} = 0, \quad \forall t \in \mathcal{T}, \quad (39)$$

$$\delta \cdot \sum_{t \in \mathcal{T}} \left(\frac{R_{DRI_h^d,t}}{\overline{\kappa}_{DRI}^{De}} \right) + \overline{w}_{Tr} \le \overline{W}_{Tr}, \quad \forall t \in \mathcal{T}, \forall h \in \mathcal{H}, \quad (40)$$

where $\overline{w}_{Tr}$ represents the transfer time, $\overline{W}_{Tr}$ is the maximum allowable time, and $\overline{\kappa}_{DRI}^{De}$ denotes the quantity of DRI transferred in one batch, measured in tonnes.

4.2.5. Boundary dependency

Boundary dependency constraints ensure seamless integration and material conservation across the H_2-DRI-EAF process. The material conservation between HP-RTN and HS-RTN is managed by (41). Hydrogen supply to DR-RTN, partially sourced from the HP process and hydrogen released from HT, is governed by (42). A constant hydrogen supply rate is maintained through (43). The material balance between the production of DRI and the demand is achieved through (44). A constant supply rate is ensured to meet the DRI demand through (45). Production requirements for each batch at the end of the process are fulfilled by (46).

$$\Pi_{H_2^{TP},t} - \Pi_{H_2^{DC},t} + \Pi_{H_2^{St},t} = 0, \quad \forall t \in \mathcal{T}, \quad (41)$$

$$\Pi_{H_2^{De},t} + \Pi_{H_2^{DC},t} + \Pi_{H_2^{Re},t} = 0, \quad \forall t \in \mathcal{T}, \quad (42)$$

$$\Pi_{H_2^{De},t} = \overline{\kappa}_{H_2}^{De} \cdot \boldsymbol{N}_{DR,t}, \quad \forall t \in \mathcal{T}, \quad (43)$$

$$\Pi_{DRI^{De},t} + \Pi_{DRI^{TP},t} = 0, \quad \forall t \in \mathcal{T}, \quad (44)$$

$$\Pi_{DRI^{De},t} = \overline{\kappa}_{DRI}^{De} \cdot \boldsymbol{N}_{Tr_h,t}, \quad \forall t \in \mathcal{T}, \quad (45)$$

$$\Pi_{LS_h,T} = -\overline{LS_h}, \quad \forall h \in \mathcal{H}, \quad (46)$$

where $\overline{\kappa}_{H_2}^{De}$ represents the constant flow rate of hydrogen fed into the SF, measured in tonnes, and $\overline{LS_h}$ indicates LS demand for each batch.

Additionally, all remaining $\Pi_{r,t}$ values should be set to zero to prevent disruptions from external inputs and outputs, as mandated in (47)–(51):

$$\Pi_{LS_h,t} = 0, \quad \forall h \in \mathcal{H}, \forall t \in \mathcal{T}_{\neg\{t=T\}}, \quad (47)$$

$$\Pi_{r,t} = 0, \quad \forall r \in \mathcal{R}^{HP}_{\neg\left\{H_2^{DC}\right\}}, \forall t \in \mathcal{T}, \quad (48)$$

$$\Pi_{r,t} = 0, \quad \forall r \in \mathcal{R}^{HS}_{\neg\left\{H_2^{Re}\right\}}, \forall t \in \mathcal{T}, \quad (49)$$

$$\Pi_{r,t} = 0, \quad \forall r \in \mathcal{R}^{DR}_{\neg\left\{H_2^{De}, DRI^{TP}\right\}}, \forall t \in \mathcal{T}, \quad (50)$$

$$\Pi_{r,t} = 0, \quad \forall r \in \mathcal{R}^{ES}_{\neg\left\{DRI^{De}, LS_h\right\}}, \forall t \in \mathcal{T}. \quad (51)$$

4.2.6. Power balance

Power balance constraints ensure the equilibrium between electricity supply and demand, which is crucial under energy constraints. It is worth noting that, after discretisation, we assume that the total electricity in each interval corresponds to its power, adhering to the following power balance constraints (52)–(55):

$$\boldsymbol{P}_{El^{Elz},t} = P_t^{G,Elz} + P_t^{WT,Elz}, \quad \forall t \in \mathcal{T}, \quad (52)$$

$$\boldsymbol{P}_{El^{EAF},t} = P_t^{G,EAF} + P_t^{WT,EAF}, \quad \forall t \in \mathcal{T}, \quad (53)$$

Table 1
Technical Parameters of the PEM Electrolyser.

Item	Nominal Power	Power Adjustable Range	Operational Efficiency	H_2 Production Rate
Value	17.5 MW	40%–100%	90%	335 kg/hour

Table 2
Technical Parameters of Hydrogen Tank.

Item	Storage Capacity	Charging/Release Flow Rate	Operational Capacity Range
Note	Max. 250 kg	Max. 105 kg H_2/hour	10%–90%

Table 3
Technical Parameters of Electric Arc Furnace.

Item	Nominal Power	Equipment Efficiency	Liquid Steel per Batch	Processing Time
Value	228 MW	80%	240 tonne	60 min

$$\boldsymbol{P}_{El^{WT},t} = P_t^{WT,Elz} + P_t^{WT,EAF} + P_t^{Cur}, \quad \forall t \in \mathcal{T}, \quad (54)$$

$$\boldsymbol{P}_{El^{PG},t} = P_t^{G,Elz} + P_t^{G,EAF}, \quad \forall t \in \mathcal{T}, \quad (55)$$

where $P_t^{G,Elz}$ and $P_t^{WT,Elz}$ represent the power sources for the PEMEL from the grid and WT, respectively, at time t. Similarly, $P_t^{G,EAF}$ and $P_t^{WT,EAF}$ denote the power sources for the EAF from the grid and WT at time t. $R_{El^{WT},t}$ refers to electricity supplied by WT at time slot t, and P_t^{Cur} indicates the electricity curtailment of WT at time t.

5. Case study

5.1. Case description

This section examines a modified HISP, referred the HYBRIT pilot project [6], using the above-ground hydrogen tank as a generic storage solution. Equipment selection and parameter settings are based on real industrial data. The technical specifications of each PEMEL array, corresponding to the Siemens product 'Silyzer 300' [28], are provided in Table 1. To ensure the required quantity of H2 for the ironmaking stage, 25 PEM electrolysis arrays are stacked. The specifications of each HT unit, as detailed in Table 2, correspond to the GKN HYDROGEN product 'HY2MEGA' [29]. Ten HT units are stacked to form an HT system for increased storage capacity. The operating range of the HT system is managed to prevent any degradation of lifespan caused by excessive release and storage. The technical specifications of the DRI shaft furnace, pertain to the MIDREX shaft furnace introduced by [30]. The technical parameters of the EAF, listed in Table 3, are associated with the DANIELI ZEROBUCKET EAF technology [31]. Based on stoichiometric principles, the mass dependencies of the H_2-DRI-EAF process are given in Table 4.

Regarding the parameter settings, a 30-min interval is adopted, which aligns with typical electricity pricing and renewable forecasts. The minimum transfer time is 30 min, and the maximum acceptable transfer duration is 360 min. The number of EAF units is 2. To meet DRI hydrogen needs, 25 PEMEL arrays are stacked to produce 4.19 tonnes per interval, and 50 HT units enhance storage capacity to 12.5 tonnes with a faster flow of 2.63 tonnes per interval. The operating range of the HT is maintained between 10% and 90% to extend its lifespan. SF produces 120 tonnes of DRI per interval, requiring 6.12 tonnes of hydrogen, and EAF processes 240 tonnes per batch in a 60-min cycle. The total demand of LS $\overline{LS_{TD}}$ is calculated by multiplying the LS capacity per batch processed in the EAF by the required number of batches.

The day-ahead wholesale electricity price profile [32], the related carbon intensity of the local power grid [33] and the wind power profiles [34] of a nearby 500 MW wind farm over a 24-h period (00:00 to 24:00) are presented in Fig. 4. The carbon price is set at £80 per tonne of CO_2 produced. The curtailment electricity price is set at £10 per MWh.

To verify the performance of cost-effective scheduling of an HISP in improving economic feasibility, case studies were conducted under two operation schemes:

(1) *OPT-Min*: The *OPT-Min* scheme serves as a baseline, reflecting the most common scheduling strategy described in [25], aimed at minimising the OPT required to complete all scheduled tasks.

(2) *Cost-Min*: The *Cost-Min* scheme focuses on minimising operational costs by leveraging flexibility during idle production times and utilising the arbitrage potential of the hydrogen storage tank to achieve cost reductions.

The proposed scheduling model features a 24-h schedule horizon with 30-min time intervals. The model was performed in Python with Gurobi 11.0 Solver [35] on a desktop powered by an Intel Core i7-11700 (2.5 GHz) processor and 16 GB of RAM running Windows 11.

5.2. Validation of the RTN-based process formulation

To ensure practical applicability, a case involving six batches of LS production under the *OPT-Min* operation scheme was used for validation. This focused on verifying the task sequence and mass balance within the H_2-DRI-EAF process.

5.2.1. Task sequence validation

The Gantt chart in Fig. 5(a) visually illustrates equipment occupancy over time, showing how resources (e.g., PEMEL, HT, SF, EAF) are utilised and highlighting task dependencies for efficient operation. For illustrative purposes, we use the production of the first batch as an example, with equipment operating states highlighted by red dashed boxes in Fig. 5(a). From 00:00 to 01:30, three batches of hydrogen are produced in the PEMEL, then stored in the HT from 00:30 to 02:00. The production of each batch of hydrogen is completed at the end of the time slot, which is immediately followed by storage in the next time slot, with no idle period in between. For example, for the first batch of hydrogen, the PEMEL equipment begins hydrogen production at 00:00 and completes it at 00:30, after which the hydrogen becomes available at 00:30. Consequently, the hydrogen storage task starts at 00:30, utilising the hydrogen immediately. This validate the compliance with constraint (35), which requires that each batch of hydrogen produced by PEMEL must be processed immediately without delay. Likewise, the similar validation applied to the subsequent tasks. From 02:30 to 03:30, iron ore is directly reduced in the SF using hydrogen produced in the PEMEL and released from HT. Then, after 30 min of transportation by the TV, the generated DRI is transported to the EAF stage at 04:00. Finally, from 04:00–05:00, DRI is further processed in the EAF for LS production. Notably, the EAF operates continuously throughout the entire batch period without interruption. Additionally, in the EAF steelmaking stage, tasks are scheduled to avoid temporal conflicts during parallel operations. For instance, when EAF_1 unit is

Table 4
Stoichiometric Balance of Each Sub-Process.

Process	Input		Output	
	Mass	Amount	Mass	Amount
Hydrogen production	Water	9 tonne	Hydrogen	1 tonne
Direct reduction	Hydrogen	0.051 tonne	Direct reduced iron	1 tonne
EAF steelmaking	Direct reduced iron	1 tonne	Liquid steel	1 tonne

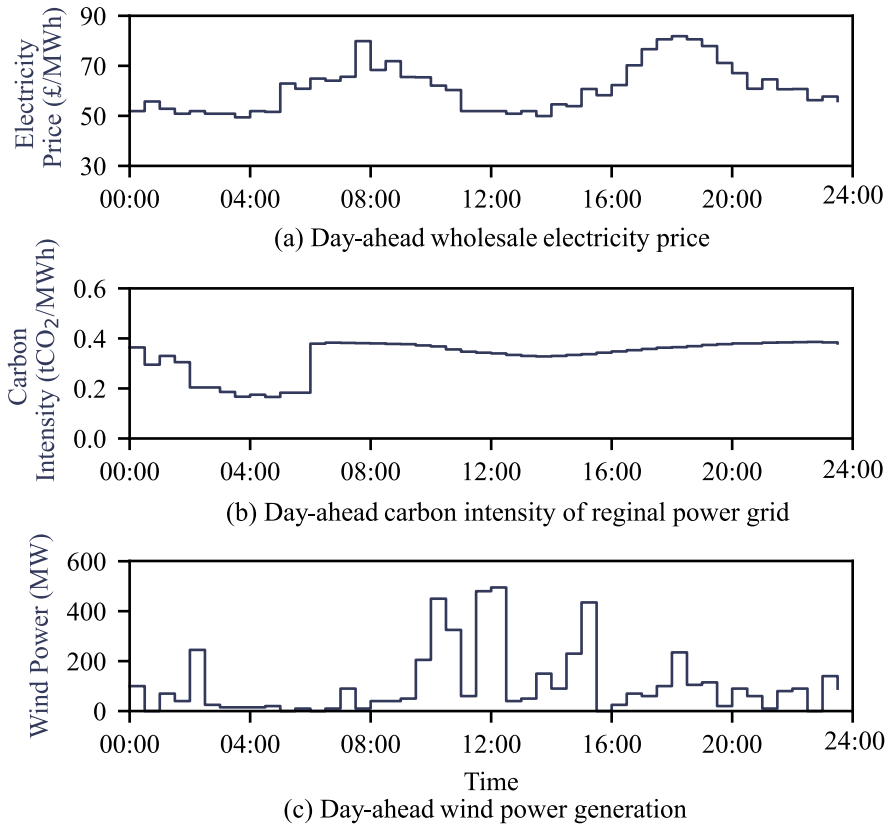

Fig. 4. Day-ahead Forcast Profiles of Wholesale Price, Carbon Intensity and Wind Power.

occupied from 07:30 to 08:00, the ES task is assigned to the other available EAF_2 unit.

Fig. 5(b) illustrates the Gantt chart under the *Cost-Min* operation scheme. Similar to the analysis of Fig. 5(a), it satisfies task sequencing validations. Compared to Fig. 5(a), the equipment operating times in Fig. 5(b) are more dispersed throughout the day, utilising idle periods to improve scheduling flexibility and reduce operational costs. Further insights into how this flexibility contributes to cost savings and grid stress alleviations are discussed in Section 5.3.

5.2.2. Mass balance validation

Mass balance under the *OPT-Min* operation scheme is illustrated in Figs. 6–8, which quantitatively validate critical dependencies between inputs and outputs, and adherence to stoichiometric balances and equipment capacities in the H_2-DRI-EAF process. For illustrative purposes, we examine the production of the first batch of LS with a capacity of 240 tonnes. Based on stoichiometric calculations, 12.24 tonnes of hydrogen are required for one batch of LS, and since the EAF operates continuously for 60 min at constant power, each time slot must provide 6.12 tonnes of hydrogen. Following the process sequence, between 00:00 and 01:30 (Fig. 6(a)), the PEMEL produces hydrogen at a rate of 2.63 tonnes per time slot. From 00:30 to 02:00 (Fig. 6(b)), this hydrogen is stored in the HT at the same rate, indicating that all hydrogen produced between 00:00 and 01:30 is fully stored in the HT. Subsequently, from 02:30 to 03:30, the SF directly reduces iron ore using hydrogen at 6.12 tonnes per time slot, of which 4.19 tonnes are produced by the PEMEL and 1.93 tonnes are released from the HT (Fig. 6(c)). The DRI generated in the SF at a rate of 120 tonnes per time slot (Fig. 7(a)) requires exactly 6.12 tonnes of hydrogen, matching the combined supply from the PEMEL and HT. Furthermore, all equipment operates within capacity limits: H_2 production is capped at 4.19 tonnes (Fig. 6(a)), the HT flow rate remains below 2.63 tonnes (Fig. 6(b)), the SF consistently processes 120 tonnes of DRI (Fig. 7(a)), and EAF produces 240 tonnes of LS per batch (Fig. 8).

5.3. Optimal scheduling under OPT-min and cost-min schemes

5.3.1. Operation costs reduction and grid stress alleviation

Table 5 shows the cost reductions achieved by the *Cost-Min* scheme at different LS production scales compared to the *OPT-Min* scheme. The *Cost-Min* scheme reduces total operational costs by up to 58.58% at the 6 batches LS production scale, including a 43% decrease in wholesale costs, a 91.3% drop in curtailment costs, and a 32.3% reduction in indirect emission costs through optimal scheduling. It is also worth noting that as production batches increase, the reduction rate drops from 58.58% at 6 batches to 3.77% at 21 batches due to the decreased flexibility in scheduling tasks caused by reduced idle time, as well as reduced arbitrage opportunities for HT.

Fig. 9 demonstrates how the *Cost-Min* operation scheme (Fig. 9(c)) optimises scheduling to alleviate grid stress, in contrast to the *OPT-Min* operation scheme (Fig. 9(b)), by comparing their purchased and

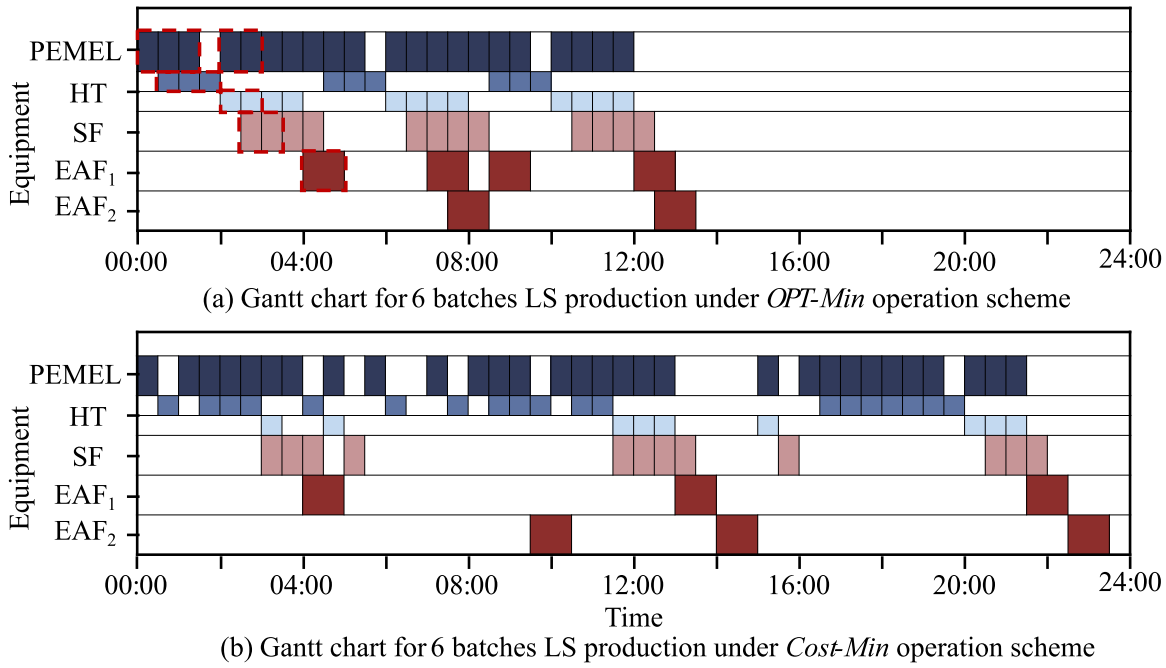

Fig. 5. Gantt Chart for 6 Batch LS Production under OPT-Min and Cost-Min Operation Schemes.

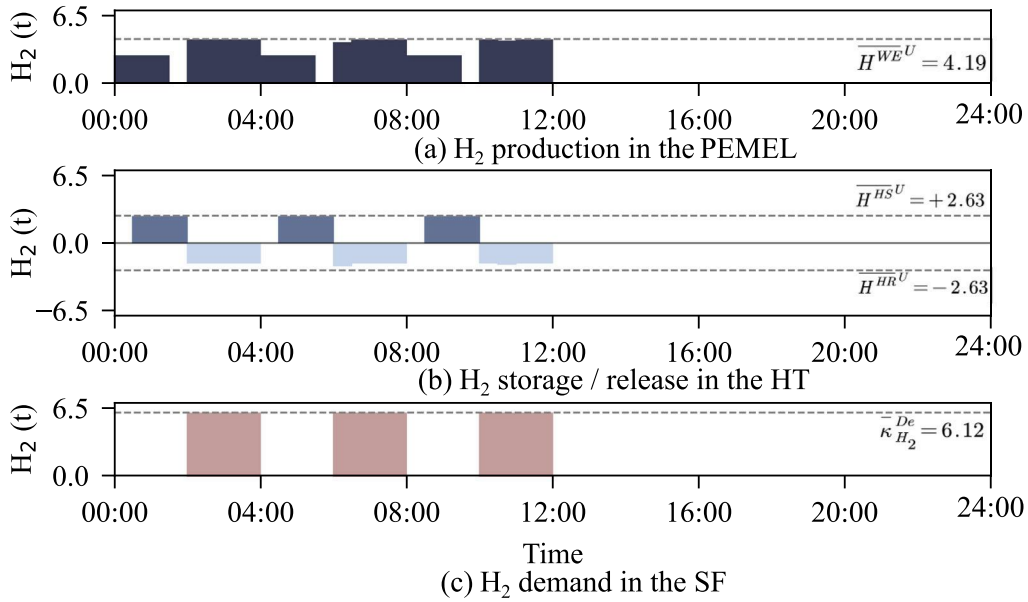

Fig. 6. Mass Dependencies of H_2 among PEMEL, HT and SF.

Table 5
Cost Comparison in Different Production Scale of Steel.

Batches	Schemes	Wholesale Cost (k£)	Curtailment Cost (k£)	Emission Cost (k£)	Total Cost (k£)
6	*OPT-Min*	264.9	177.6	91.3	533.8
	Cost-Min	151.0	8.4	61.8	221.1
10	*OPT-Min*	467.8	143.2	179.6	790.5
	Cost-Min	344.6	10.7	131.9	487.1
16	*OPT-Min*	693.3	45.4	287.4	1026.1
	Cost-Min	635.7	3.6	267.7	907.0
21	*OPT-Min*	967.9	9.2	405.3	1382.4
	Cost-Min	929.5	3.6	397.2	1330.3

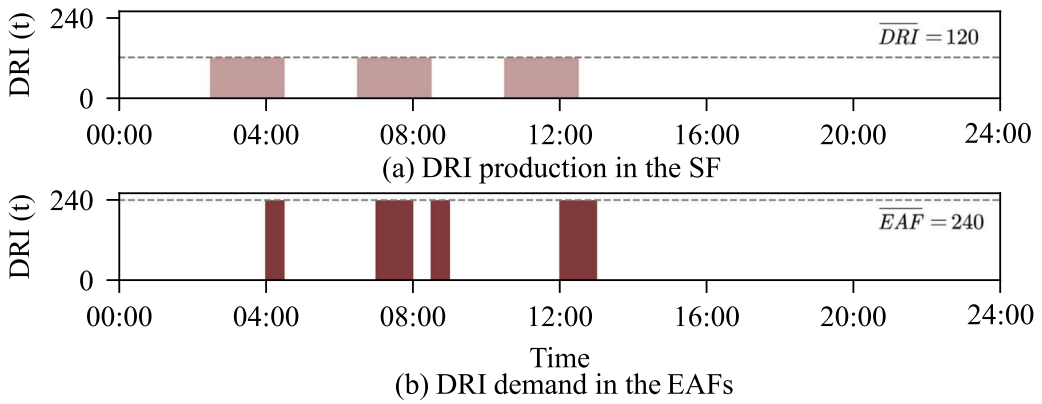

Fig. 7. Mass Dependencies of DRI between SF and EAFs.

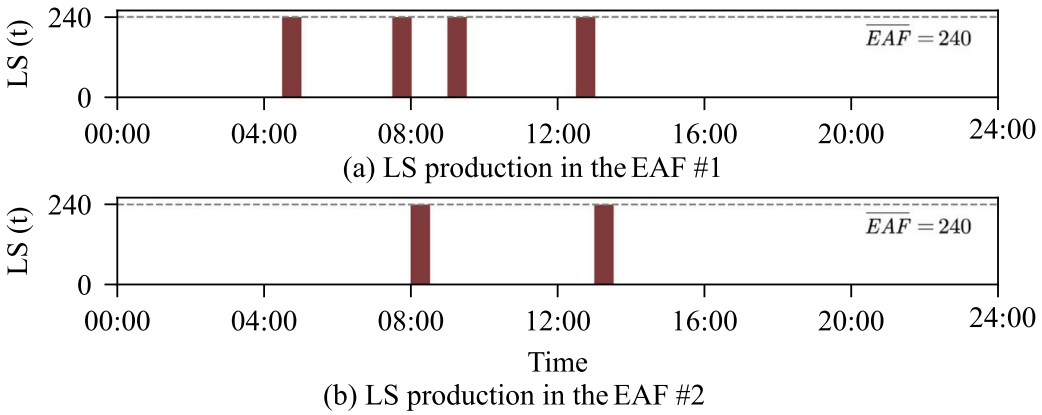

Fig. 8. Mass Dependencies of LS between Two Parallel EAFs.

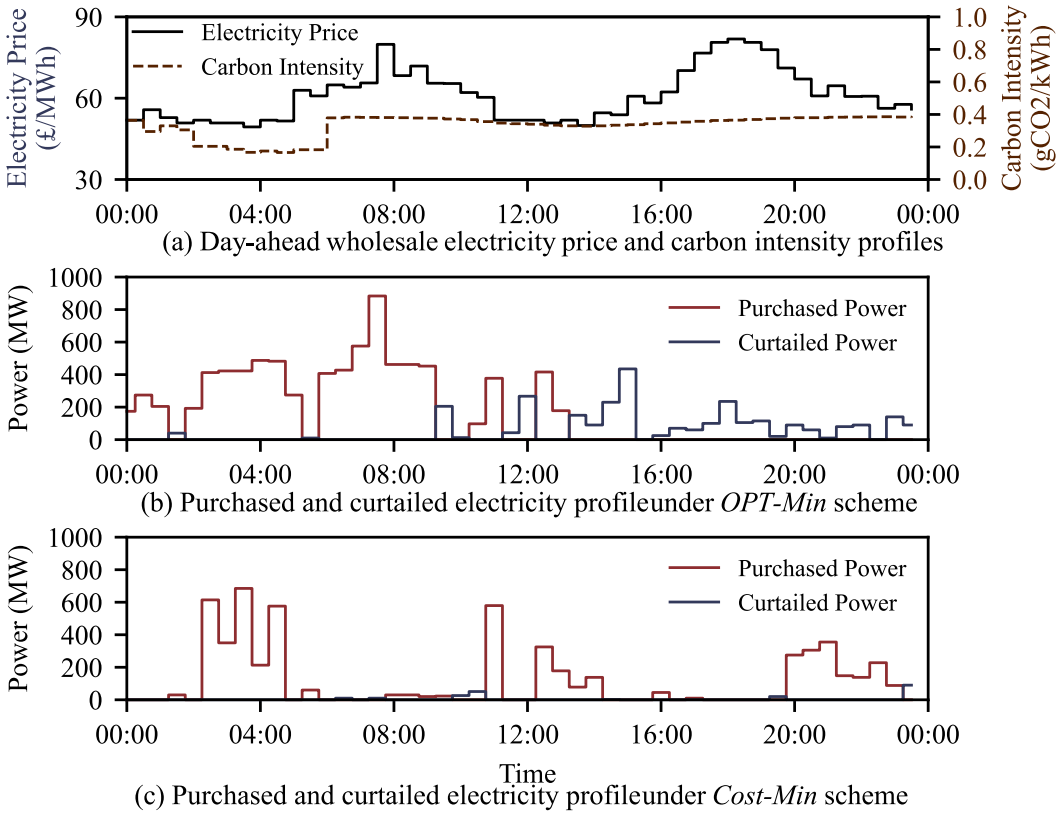

Fig. 9. Comparisons of Purchased and Curtailed Electricity under *OPT-Min* and *Cost-Min* Schemes.

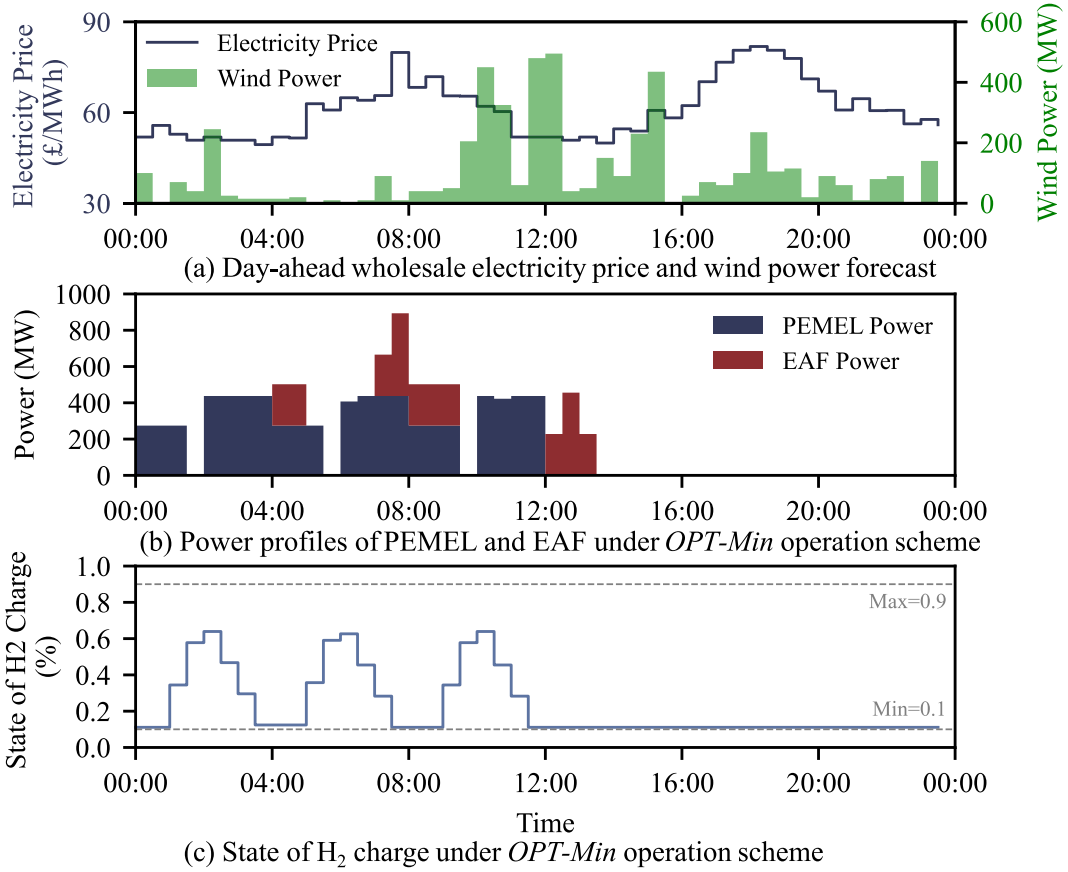

Fig. 10. Load Power Profiles and SoHC under *OPT-Min* Operation Scheme.

curtailed power profiles. The *Cost-Min* operation scheme effectively reduces the peak load by 22.5%, from 884 to 685 MW, by redistributing loads to periods such as 02:00 to 04:30 and 11:00 to 11:30 when electricity prices and CI are notably lower. These strategic shifts not only decrease wholesale and emission costs, but also significantly reduce curtailment costs by 92.5%, further facilitating the integration of renewable energy into the grid.

5.3.2. Optimal schedules of h_2-DRI-EAF process

To illustrate how flexibility in the H_2-DRI-EAF process contributes to cost reductions, load power profiles and state of the H_2 charge (SoHC) of HT under the *OPT-Min* (Fig. 10) and *Cost-Min* (Fig. 11) operation schemes are compared. The power profiles of PEMEL and EAF under *OPT-Min* and *Cost-Min* operation scheme are illustrated in Figs. 10(b) and 11(b), respectively. Compared with schedules under the *OPT-Min* operation scheme, the *Cost-Min* operation scheme strategically schedules the timing and power consumption for PEMEL and EAF to minimise operational costs. During peak electricity price period from 05:00 to 09:00, the *Cost-Min* scheme reduces power usage for these processes and shifts it to lower electricity price periods. Additionally, HT utilises arbitrage by storing hydrogen during periods with excess wind power from 17:00 and 19:30, thus optimising energy use and reducing wind power curtailment. The SoHC, defined as the hydrogen amount in HT to its rated capacity, remains within 10%–90% limits under the *OPT-Min* (Fig. 10(c)) and *Cost-Min* (Fig. 11(c)) operation schemes.

6. Conclusion

In this paper, a cost-effective scheduling model is proposed for HISPs, which are powered by a grid-assisted renewable energy system, to enhance their economic feasibility. Individual RTN model is initially developed for each HISP sub-process to represent its distinct operational characteristics. These individual RTN models are subsequently integrated using boundary dependency constraints that capture the coupling between HISP sub-processes. The resulting integrated RTN model is then incorporated into the optimisation framework to enable cost-effective scheduling of HISPs. In case studies, the integrated RTN model is first validated from the perspectives of task sequence and mass balance. To evaluate the performance of the proposed cost-effective scheduling model, results of the *OPT-Min* and the *Cost-Min* schemes are compared and analysed, showing the effectiveness of the proposed method in improving HISP economic feasibility. The results indicate that the cost-effective schedule under the *Cost-Min* scheme reduces the total operational cost by up to 58.58% compared to the *OPT-Min* scheme. Furthermore, cost reductions of the HISP are observed across various production scales, implying the potential of the proposed method to support the commercialisation of HISP.

Prospective improvement of our work will focus on two main areas. First, we aim to integrate our proposed method to a dynamic rescheduling framework and investigate the fast—solving of rescheduling problems to improves the economic efficiency of HISPs in the intraday stage. With appropriate modifications, this extension will effectively handle differences between day-ahead plans and actual production when rescheduling is necessary. Second, the proposed model will be integrated into the steel plant's existing manufacturing execution system as a dedicated functional module. This integration will involve collaboration closely with both the steel plant operators and the manufacturing execution system developers to ensure seamless alignment with operational practices while remaining an intuitive and user-friendly interface, thereby minimising potential barriers to successful adoption within the existing production environment.

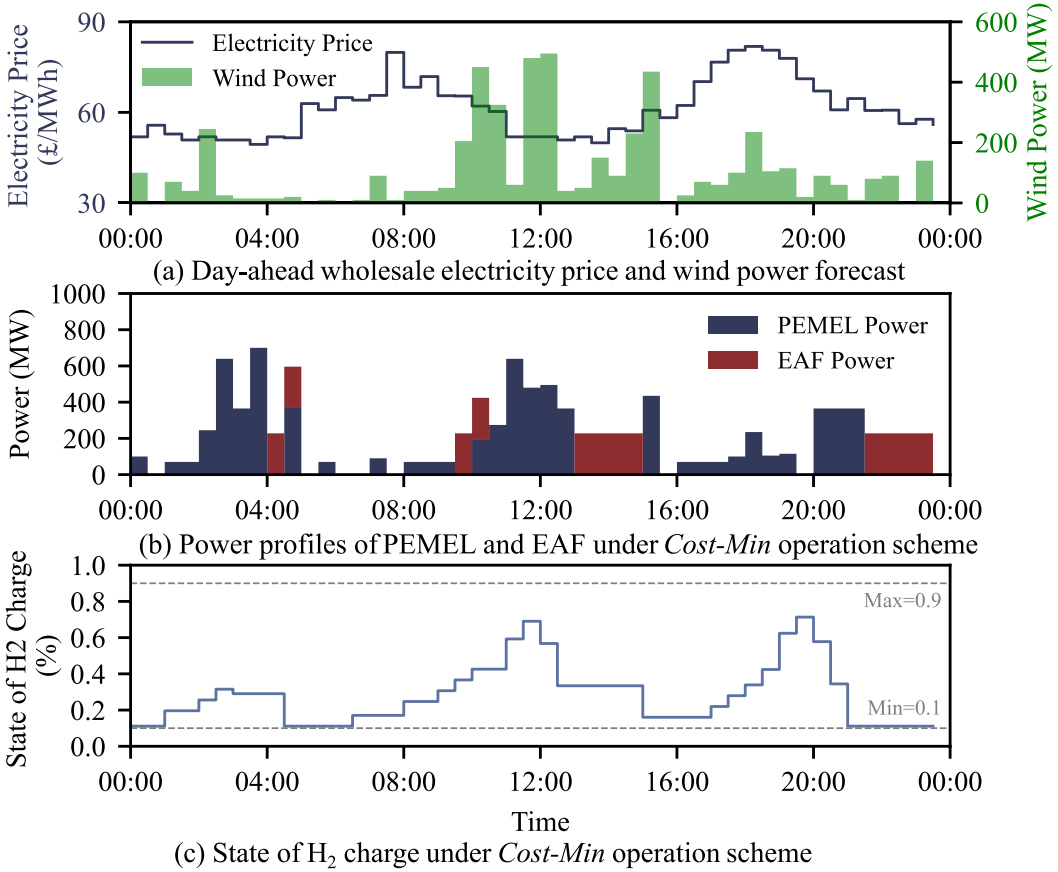

Fig. 11. Load Power Profiles and SoHC under *Cost-Min* Operation Scheme.

CRediT authorship contribution statement

Pengfei Su: Writing – original draft, Writing – review & editing, Visualization, Software, Methodology, Investigation, Conceptualization. **Yue Zhou:** Writing – review & editing, Supervision, Resources, Project administration, Conceptualization. **Hongyi Li:** Writing – review & editing, Conceptualization. **Hector D. Perez:** Writing – review & editing, Methodology. **Jianzhong Wu:** Writing – review & editing, Supervision, Resources, Project administration, Conceptualization.

Declaration of competing interest

The authors declare that they have no known competing financial interests or personal relationships that could have appeared to influence the work reported in this paper.

Acknowledgements

This work was supported by the China Scholarship Council, China and EPSRC, United Kingdom, through the projects EP/T021969/1 (MC2), EP /W028573/1 (Digital Twin with Data-Driven Predictive Control: Unlocking Flexibility of Industrial Plants for Supporting a Net Zero Electricity System), and SFSC2-203 (Smart and Flexible Operation of Steelmaking Plants in a Net-Zero Electricity System – A Digital Twin Approach) as a feasibility study funded by EP/S018107/1 (SUSTAIN Manufacturing Hub).

Data availability

Information on the data underpinning the results presented here, including how to access them, can be found in the Cardiff University data catalogue at 10.17035/cardiff.28359110.

References

[1] International Energy Agency (IEA). Iron and steel technology roadmap. Towards more sustainable steelmaking. tech. rep., Paris: IEA; 2020.
[2] Superchi F, Mati A, Carcasci C, Bianchini A. Techno-economic analysis of wind-powered green hydrogen production to facilitate the decarbonization of hard-to-abate sectors: A case study on steelmaking. Appl Energ 2023;342:121198.
[3] Lei T, Wang D, Yu X, Ma S, Zhao W, Cui C, Meng J, Tao S, Guan D. Global iron and steel plant CO2 emissions and carbon-neutrality pathways. Nature 2023;622(7983):514–20.
[4] Devlin A, Kossen J, Goldie-Jones H, Yang A. Global green hydrogen-based steel opportunities surrounding high quality renewable energy and iron ore deposits. Nature Commun 2023;14(1):2578.
[5] LeadIT. Green steel tracker. 2024, [Online]. Available: https://www.industrytransition.org/green-steel-tracker/.
[6] Hybrit. Hybrit: fossil-free steel. 2024, [Online]. Available: https://www.hybritdevelopment.se/en/.
[7] Devlin A, Yang A. Regional supply chains for decarbonising steel: Energy efficiency and green premium mitigation. Energy Convers Manage 2022;254:115268.
[8] Toktarova A, Walter V, Göransson L, Johnsson F. Interaction between electrified steel production and the north European electricity system. Appl Energy 2022;310:118584.
[9] Papadaskalopoulos D, Moreira R, Strbac G, Pudjianto D, Djapic P, Teng F, et al. Quantifying the potential economic benefits of flexible industrial demand in the European power system. IEEE Trans Ind Inf 2018;14(11):5123–32.
[10] Zhang X, Hug G, Harjunkoski I. Cost-effective scheduling of steel plants with flexible EAFs. IEEE Trans Smart Grid 2017;8(1):239–49.
[11] Gan L, Yang T, Chen X, Li G, Yu K. Purchased power dispatching potential evaluation of steel plant with joint multienergy system and production process optimization. IEEE Trans Ind Appl 2022;58(2):1581–91 .
[12] Huang X, Hong SH, Li Y. Hour-ahead price based energy management scheme for industrial facilities. IEEE Trans Ind Inf 2017;13(6):2886–98.
[13] Zhou Y, Cheng M, Wu J. Enhanced frequency response from industrial heating loads for electric power systems. IEEE Trans Ind Inf 2019;15(6):3388–99.
[14] Zhao N, Yue D, Dou C, Shi T. Distributed dynamic event-triggered cooperative control of multiple TCLs and HESS for improving frequency regulation. IEEE Trans Ind Inf 2024;20(2):1539–49.

[15] Palensky P, Dietrich D. Demand side management: Demand response, intelligent energy systems, and smart loads. IEEE Trans Ind Inf 2011;7(3):381–8.
[16] Al-Worafi YM. Barriers of simulation research. In: Al-Worafi YM, editor. Comprehensive healthcare simulation: pharmacy education, practice and research. Cham: Springer International Publishing; 2023, p. 273–6.
[17] Castro PM, Grossmann IE, Zhang Q. Expanding scope and computational challenges in process scheduling. Comput Chem Eng 2018;114:14–42.
[18] Elsheikh H, Eveloy V. Renewable hydrogen based direct iron ore reduction and steel making with grid assistance. Energy Convers Manage 2023;297:117544.
[19] Deng J, Sierla S, Sun J, Vyatkin V. Reinforcement learning for industrial process control: A case study in flatness control in steel industry. Comput Ind 2022;143:103748.
[20] Che G, Zhang Y, Tang L, Zhao S. A deep reinforcement learning based multi-objective optimization for the scheduling of oxygen production system in integrated iron and steel plants. Appl Energy 2023;345:121332.
[21] Li L, Yang X, Yang S, Xu X. Optimization of oxygen system scheduling in hybrid action space based on deep reinforcement learning. Comput Chem Eng 2023;171:108168.
[22] Pantelides CC. Unified frameworks for optimal process planning and scheduling. In: Proceedings on the second conference on foundations of computer aided operations. Cache Publications New York; 1994, p. 253–74.
[23] Perez HD, Amaran S, Iyer SS, Wassick JM, Grossmann IE. Chapter 14 - applications of the RTN scheduling model in the chemical industry. In: Bortz M, Asprion N, editors. Simulation and optimization in process engineering. Elsevier; 2022, p. 365–400.
[24] Castro PM, Sun L, Harjunkoski I. Resource–task network formulations for industrial demand side management of a steel plant. Ind Eng Chem Res 2013;52(36):13046–58.
[25] Su P, Zhou Y, Wu J. Multi-objective scheduling of a steelmaking plant integrated with renewable energy sources and energy storage systems: Balancing costs, emissions and make-span. J Clean Prod 2023;428:139350.
[26] Wang J, Wang Q, Sun W. Optimal power system flexibility-based scheduling in iron and steel production: A case of steelmaking–refining–continuous casting process. J Clean Prod 2023;414:137619.
[27] Ali S, Sun H, Zhao Y. Model learning: a survey of foundations, tools and applications. Front Comput Sci 2021;15(5):155210.
[28] Siemens-Energy. Green hydrogen production. 2024, https://www.siemens-energy.com/global/en/home/products-services/product-offerings/hydrogen-solutions.html.
[29] Hydrogen G. Hydrogen storage all-in-one-solutions. 2024, https://www.gknhydrogen.com/product/,
[30] MIDREX Technologies, Inc. Direct from MIDREX. https://www.midrex.com/tech-article/midrex-direct-reduction-plants-2022-operations-summary/.
[31] DANIELI. Electric Arc Furnaces, https://www.danieli.com/en/products/products-processes-and-technologies/electric-arc-furnace_26_83.htm.
[32] Energy Stats UK. Historical pricing data from octopus energy tariffs. 2024, [Online]. Available: https://energy-stats.uk/,
[33] National Grid ESO. Carbon intensity API. 2023, [Online]. Available: https://carbonintensity.org.uk/.
[34] Bassi W, Rodrigues AL, Sauer IL. Implantation, operation data and performance assessment of an urban area grid-connected small wind turbine. Wind 2022;2(4):711–32.
[35] Gurobi Optimization, LLC. Gurobi optimizer reference manual. 2024, [Online]. Available: https://www.gurobi.com.